Published in final edited form as:
Alzheimers Dement. 2010 January ; 6(1): 54. doi:10.1016/j.jalz.2009.04.1228.

White matter integrity and cortical metabolic associations in aging and dementia

B. Kuczynski[1], **E. Targan**[1], **C. Madison**[1], **M. Weiner**[3], **Y. Zhang**[3], **B. Reed**[2], **HC. Chui**[4], and **W. Jagust**[1]

[1] Helen Wills Neuroscience Institute, University of California, Berkeley, and the Lawrence Berkeley National Laboratory, University of California

[2] Davis, Alzheimer's Center and Northern California Veterans Affairs Health Care System, University of California, San Francisco

[3] Department of Veterans Affairs Medical Center, University of Southern California, Los Angeles

[4] Department of Neurology, University of Southern California, Los Angeles

Abstract

Background—Studies show white matter hyperintensities, regardless of location, primarily affect frontal lobe metabolism and function. This report investigates how regional white matter integrity (measured as fractional anisotropy (FA)) relates to brain metabolism in order to unravel the complex relationship between white matter change and brain metabolism.

Objective—To elucidate the relationship between white matter integrity and gray matter metabolism using diffusion tensor imaging (DTI) and fluorodeoxyglucose-positron emission tomography (FDG-PET) in a cohort of 16 subjects ranging from normal to demented (age>55).

Methods—Cross-sectional regression analyses using mean FA values from white matter regions underlying the medial prefrontal, inferior-lateral prefrontal, parietal association, and posterior temporal areas and corpus callosum were regressed with glucose metabolism (PET) using SPM2 ($p < 0.005$, voxel cluster > 100). Regional cerebral glucose metabolism was the primary outcome measure, with our major hypotheses being those hypometabolic cortical regions affected by Alzheimer's disease would correlate with lower FA of associated tracks.

Results—Our data show inter-regional positive correlations between FA and gray matter metabolism for the prefrontal cortex, temporal and parietal regions. Our results suggest left prefrontal FA is associated with left temporal and parietal metabolism. Further, left posterior temporal FA correlated with left prefrontal metabolism. Finally, bilateral parietal FA correlated with bilateral temporal metabolism.

Conclusions—These regions are associated with the cognitive processes affected in AD and Cerebrovascular Disease, suggesting a link with white matter degeneration and gray matter

Address correspondence and reprint requests to Dr. Beth Kuczynski, University of California, Helen Wills Neuroscience Institute, 118 Barker Hall MC 3190, Berkeley, CA 94720; phone: 925-708-0560, fax: 510-642-3192, e-mail: beth.kuczynski@gmail.com.

Disclosure Statement

There are no actual or potential conflicts of interest in this study.

hypometabolism. Therefore cortical function and white matter degeneration are related in aging and dementia.

Keywords

PET; DTI; FA; metabolism; white matter; dementia; Alzheimers disease

1. Introduction

Alzheimer's disease (AD) and cerebrovascular disease (CVD) are the primary causes of dementia in the elderly population. AD and CVD are often concomitant and discerning which is the major cause of dementia may be quite complex. Both diseases are associated with atrophy, hypometabolism, white matter degradation and cognitive decline. The relationship between white matter alterations and brain function within the elderly has been investigated to some degree. Imaging studies show that white matter hyperintensities (WMH), regardless of location, are associated with both global and frontal lobe brain alterations. Specifically, white matter lesions are associated with total brain atrophy [1], frontal lobe hypometabolism and impaired executive function [2,3], and diminished prefrontal cortical activation and cognition [4].

Classification of tissue as WMH is generally accomplished using segmentation methods that yield binary information. However, characterizing white matter integrity via WMH does not fully capture the range of white matter degradation that may be present in the aging brain. Diffusion tensor imaging (DTI) measures integrity of white matter fibers through a number of quantitative methods, including calculation of fractional anisotropy (FA). DTI studies of aging reveal lower fractional anisotropic values in a number of brain regions. Age-related studies of normal populations report white matter degeneration occurring in the frontal lobe and anterior corpus callosum, with the temporal and parietal regions spared [5,6]. However, studies focusing on AD find compromised white matter integrity within the posterior cingulate, corpus callosum, temporal, and parietal regions [7–13]. Interestingly, the decrease in white matter integrity within AD appears to correspond to those regions most affected metabolically. Positron emission tomography (PET) studies of glucose metabolism in AD consistently report hypometabolism within the posterior cingulate, temporo-parietal regions and some reports find the dorsal and ventral lateral frontal regions affected as well [14–19]. In addition to the well-known cortical regions associated with AD, subcortical structures such as the thalamus and putamen (regions proximal to the lacunar infarcts commonly found in AD) also indicate atrophy [20] and hypometabolism [21].

Our goal was to investigate the relationship between white matter integrity and brain metabolism using regional FA and cortical metabolism via DTI and PET, respectively, in a cohort of cognitively normal, impaired not demented and demented individuals. Within this study, we are attempting to understand the complex relationship between white matter change and brain metabolism by focusing on white matter integrity (FA) rather than WMH volume. As fibers lose integrity, an increase in isotropic diffusion of water molecules should produce a corresponding lower FA. In turn, we expect to find relationships between changes in white matter and glucose metabolism, measured with PET scanning and the tracer [18F] Flurodeoxyglucose, that reflect a loss of functional connectivity maintained by these white matter tracts. Our overall hypothesis is that the white matter underlying those cortical regions known to be metabolically affected by Alzheimer's disease will have lower white matter integrity and thus correlate with lower metabolism in associated cortical regions. Therefore, our white matter regions of interest (ROI) included those corresponding to the prefrontal regions [medial prefrontal white matter (MFWM) and inferior-lateral prefrontal white matter (IFWM)], posterior temporal regions, parietal association regions (primarily focusing on

inferior and superior parietal white matter), and the corpus callosum (splenium, body and anterior portions). We hypothesized that lower FA of these white matter ROI's would correlate with decreased metabolism of associated cortical regions, with specific emphasis on the those regions proximal to the longitudinal fasciculus, (a large bundle connecting the parietal with temporal and frontal regions). More specifically, we anticipated unilateral positive correlations indicating associations of lower temporal FA with lower metabolism in the temporal and parietal areas. Additionally, we expected lower parietal white matter FA to positively correlate with parietal, temporal and possibly frontal gray matter metabolism. Further, we expected the prefrontal white matter FA to positively correlate with prefrontal and temporal metabolism, based on fronto-temporal connectivity studies [21–25]. Finally, we expected the callosal fibers to have positive associations with proximal metabolic regions (i.e. splenium with posterior brain regions, body with medial areas and anterior fibers with more frontal regions)

2. Methods

2.1. Subjects

Sixteen subjects recruited from either the UC Davis or UCSF dementia centers between 2003 and 2005 were evaluated under the multi-institutional study of "The Aging Brain: Vasculature, Ischemia, and Behavior" having completed PET and DTI imaging sessions (mean interval between scans 0.55 years, median 0.25 years). This project is designed to detect the vascular contributions to dementia including the relationships between AD and vascular disease. Subjects were recruited in order to enrich the sample for subcortical lacunar infarction and WMH [26,27], while excluding those with cortical infarcts at entry. Informed consent to participate in the study was obtained in accordance with the policies of each institutional review board. The recruitment criteria included being above the age of 55, and between cognitively normal and moderate dementia; assessed by the Clinical Dementia Rating (CDR) score [28] of 0 to 1, with scores of 0 indicating normal cognitive function, 0.5 cognitively impaired not demented (CIND), and 1 demented. Exclusionary criteria included diagnosis of cortical stroke or other neurological illnesses (other than subcortical CVD or AD), Mini Mental State Exam (MMSE) score below 15, and the use of psychoactive drugs (other than stable doses of acetylcholinesterase inhibitors or selective serotonin reuptake inhibitors). All individuals were evaluated by clinicians at the University dementia clinics using standard criteria for Vascular Dementia [29] and Alzheimer's Disease [30].

2.2. Design

We used a regression approach including all subjects without regard to diagnostic grouping based on the observation that the pathologies of CVD and AD are both distributed in a continuous fashion with extensively overlapping distributions in this cohort [31]. Regional white matter integrity was measured using regions of interest (ROIs) drawn on the high-resolution T1 MR image, as described below. The DTI image was coregistered to the T1 and the FA values were extracted. The FA values for each ROI were then regressed with corresponding PET scans with handedness, age and MMSE controlled for in the SPM2 design as nuisance variables.

2.3. Imaging

The FDG-PET data were acquired using a Siemens-CTI ECAT EXACT (model 921), 47-slice scanner in 2D-acquisition mode to image the [18F]fluorodeoxyglucose (FDG) radiotracer. The scanner has a resolution of approximately 6 mm full-width, half-maximum (FWHM) at center to 7.5 mm tangentially and 9.6 mm radially (at 20 cm), with an axial resolution of 5 mm at the center and 8.1 mm FWHM at R=20. The axial field of the scanner is 16.2 cm and the sensitivity is 216 kcps/mCi/ml for a 20 cm cylinder phantom in 2D.

The injected dose for each individual was approximately 10 mCi of FDG. Post injection, the individual was seated in a room for 40 minutes. Subjects were then positioned in the scanner to enable a field of view encompassing the entire brain. Emission data were collected in 2D for 40 minutes, followed by a 20 min transmission period using a rotating ^{68}Ge source.

All PET scans were partial volume corrected prior to analyses. The partial volume correction involved creating a brain mask from the high resolution T1 MRI consisting of gray and white matter. Convolving this brain mask with the point spread function specific to the PET scanner provides a means for calculating the percentage of brain tissue emitting tracer at each voxel, thus eliminating the effects of CSF. The PET count for each voxel was thus adjusted based on the percent of brain matter [32]. Individual PET images were coregistered and aligned in standardized space, intensity normalized to the mean global activity and smoothed to 16 mm FWHM. Because the anatomy of the aged brain presents spatial normalization problems due to atrophy that distorts topography and makes superposition of identical regions difficult, we used a minimal deformation template (MDT2) derived from a group of aged brains [4] as the target image. The MDT2 template was created using the T1-weighted images of 25 normal, older individuals with a mean age of 71 and is described elsewhere [33].

All MRI data for this study were acquired on a 1.5 Tesla Siemens Vision MRI system. Sequences included a double spin echo with repetition time (TR)/echo time (TE)1/TE2 (5000/20/80 ms), 1 excitation, 3mm slice thickness with no slice gap, and in-plane resolution 1.25 × 1 mm^2. The second sequence provided the T1 weighted images via a T1 coronal MP-RAGE spin echo axial design (TR/TE = 10/7 ms; 1 NEX), 1 × 1 mm^2 in-plane resolution with contiguous 1.4 mm thick slices. DTI was performed using an inversion-prepared double refocused single-shot echoplanar imaging (EPI) sequence [TR/TE/inversion time(TI) = 6000/100/2000 msec] with 2.34 × 2.34 mm^2 in-plane resolution, 19 contiguous, each 5 mm thick, using a bipolar diffusion sensitizing gradient of b = 1000 s/mm^2 applied along six directions. Additional spin-echo EPI scans without diffusion gradients (b = 0) were also acquired for normalizing the diffusion measurements. Inversion recovery reduced CSF contributions and the double-refocusing RF pulses with bipolar gradients reduced the geometric distortions in the DTI. Post-processing of DTI data was implemented using DTIstudio V2 software [34] (Johns Hopkins University, Baltimore, MD) in which the analyze FA images were created.

2.4. Regions of interest

All white matter ROI's were drawn on the high-resolution T1 image. Figure 1 displays the white matter regions drawn for one individual in our cohort. Specific gyri were used as boundaries in which the underlying white matter was included for each region. The white matter of the prefrontal cortex was separated into inferior and medial prefrontal regions (IFWM and MFWM) by selecting white matter underlying the middle and inferior frontal gryi. The frontal regions were primarily drawn on the sagittal view using the axial view for additional landmarks. The IFWM (Figure 1a and c) constituted the frontal inferior opercular and triangular regions (underlying Broadman Areas (BA) 44 and 45, respectively; comprised of 10 axial slices). The posterior and superior boundaries for the IFWM, proximal to the opercularis region, were the middle frontal and precentral gyri. The axial view was used to confirm our sagittal boundaries. The final inferior axial slices included white matter subtending some insular cortex and extended superiorly to the head of the caudate. Finally, the inferior frontal sulcus, separating the IFWM and MFWM, and the inferior and midfrontal orbital gyri were used to confirm our anterior boundaries. The MFWM (Figure 1a and b), which primarily contained the middle frontal gyrus (BA 46 and 9; comprised 20 axial slices), was bordered by the inferior frontal sulcus, precentral gyrus, and the midfrontal orbital gyrus. Care was taken to avoid the cingulum area and to ensure the IFWM and MFWM did not overlap. The posterior temporal and parietal

ROI's were drawn on the coronal view. The posterior temporal region (Figure 1a,b and f), comprising the inferior, middle and superior regions not including the hippocampal region, was 20 coronal slices. The hippocampus was in view and care was taken not to include the parahippocampal region in our posterior slices. Our superior and inferior borders were the Sylvian Fissure and cerebellar cortex, respectively. The parietal association region (Figure 1a and e) was 8 coronal slices, beginning with the most posterior temporal region. The parietal region included white matter of the angular gyrus, and the inferior and superior parietal regions. Proceeding posteriorly, the region above the ventricles and Sylvian Fissure was designated parietal lobe. The medial boundary was the sulcus separating the superior parietal gyrus from the precuneus region. Finally, the corpus callosum was drawn on the sagittal view using the axial view to ensure the removal of cingulate areas. The corpus callosum (Figure 1d) was divided into the anterior, body and splenium portions using a similar technique as Hanyu et al. 1999 [8]. Briefly, the corpus callosum was split into three regions by drawing two lines at the anterior and posterior curvatures. The emergence of the caudate on the sagittal view was the lateral border. The entire corpus callosum region consisted of 18 sagittal slices. Each ROI was drawn by a single investigator (reliability < 1.0% SEM). The high resolution (T1) MRI segmented white matter was used to mask each ROI to ensure the removal of gray matter contamination. The white matter masked ROI's were then overlaid to the coregistered DTI image and the FA values were extracted. Individual FA values were used as covariates and regressed with the corresponding PET scan.

2.5. Statistical analyses

Voxel wise correlational analyses were performed on the PET data using statistical parametric mapping software (http://www.fil.ion.ucl.ac.uk/spm/). In a series of regression analyses, the FA values for each region (i.e. temporal left and right hemispheres, independently) were used as a covariate of interest and the normalized metabolic (PET) activity in each voxel was the dependent variable; while handedness, age, and MMSE were controlled for as nuisance variables in the SPM2 design. Regional associations were deemed significant if the *t*-statistic reached $p<0.005$ (uncorrected for multiple comparisons) with a cluster size > 100. The resulting significant areas were overlaid on the MDT2 template for viewing.

3.0 Results

All data are presented in radiologic format. Table 1 displays the baseline demographics for each group. As a whole, the group was well educated and only moderately cognitively impaired. By classification, those in the demented group had significantly lower baseline MMSE scores compared to the cognitively impaired not demented (CIND) and cognitively normal (CN) groups. There were no significant differences between groups for age or education. For the metabolic results below, please see Tables 2 and 3 for all significant metabolic regions showing unilateral positive associations with the lobar white matter regions and the corpus callosum, respectively, and their corresponding Montreal Neurologic Institute (MNI) coordinates.

3.1. Frontal region

Prefrontal white matter FA positively correlated with temporal and parietal metabolism. Left MFWM FA positively correlated with metabolism in the left middle occipital, superior temporal, insula, angular, and supramarginal gyri, while the right MFWM FA was solely positively associated with the metabolic pattern of the right cuneus. Left IFWM FA positively correlated with the metabolic regions of the left temporal (parahippocampal and lingual gyri), angular and middle occipital gyri. No unilateral associations were found for the right IFWM.

3.2. Posterior temporal region

Left posterior temporal regional white matter FA positively correlated with metabolism in the left frontal inferior opercularis, insula, and thalamus. Additionally, the right posterior temporal FA was positively associated with metabolism in the right cuneus and superior occipital regions. The relationships between the left IFWM (which included the white matter underlying the left inferior opercularis) and the left temporal region are shown in Figures 2a and b.

3.3. Parietal association region

The left parietal white matter FA positively correlated to metabolism in the left parahippocampal gyrus, insula, supramarginal gyrus, calcarine, precuneus, lingual and thalamic areas. Figure 2c displays some of the regions significantly associated with left parietal FA (lingual, parahippocampal and supramarginal regions). The right parietal regional FA was positively associated with right thalamic, cuneus, hippocampus, and parahippocampal regional metabolism.

3.4. Corpus callosum

Table 3 displays all significant regions associated (positive correlations) with the corpus callosum. The left anterior portion (FA) correlated with metabolism in the left calcarine, and lingual regions. There were no significant results for right anterior corpus callosum. The FA within the left posterior portion (splenium) of the corpus callosum positively correlated with the metabolic patterns in the left paracentral lobule, rolandic, insula, and small regions in the superior temporal lobe adjacent to the rolandic opercularis region and the superior frontal gyrus. The right splenium FA positively correlated to metabolism in the right hippocampus, parahippocampal, lingual, and precentral and postcentral regions. Finally the FA within the right hemispheric body of the corpus callosum positively correlated to metabolism is the right thalamus, hippocampus, and calcarine regions, while the FA of the left body fibers were positively associated to small metabolic regions within the left precentral and postcentral gyri.

3.5. Global white matter

To investigate global white matter integrity, we regressed the mean FA value for whole brain white matter via the segmented white matter mask (data not shown) with the PET data. Again, we observed left hemisphere dominance with the left superior temporal, insula, lingual, parahippocampal, calcarine, occipital, angular, supramarginal and thalamic regions showing positive metabolic associations with global FA integrity. The right hemispheric metabolic regions positively associated with global FA were the cuneus, occipital, hippocampus and parahippocampus.

3.6. Group FA differences

Although our group numbers were small, we did statistically compare (ANOVA) the extracted FA values (each white matter ROI and global FA value) across groups (data not shown). We found significant differences for the anterior bilateral corpus callosum (Demented < CIND =Normal, $p \leq 0.05$) and the right MFWM (CIND > Demented, $p<0.05$). The left MFWM showed a similar trend as the right MFWM, however it did not reach a significant threshold ($p=0.09$). There was a trend across most of the ROI's for the FA value to decrease with dementia (Normal > CIND > Demented), which was less evident in the global FA measures.

3.7. FDG-PET regressed with MMSE

In order to investigate whether hypometabolism was related to diagnosis within this cohort, we ran a voxel-wise regression analysis using SPM2 to investigate the association between metabolism and MMSE. As displayed in Figure 3, there is an association between

hypometabolism and lower MMSE score that is accentuated in the left hemisphere, although both hemispheres are affected. The regions shown are primarily those associated with AD: bilateral temporoparietal and left prefrontal cortical regions ($p < 0.001$, uncorrected for multiple comparisons; cluster > 100).

4. Discussion

We have previously shown that WMH, regardless of location, primarily affect frontal lobe metabolism and function [3]. This study was designed to elucidate the relationship between regional white matter integrity and metabolism. Our data show inter-regional positive correlations between FA and gray matter metabolism in the prefrontal, temporal and parietal regions. Our results suggest left prefrontal FA (MFWM and IFWM) is associated with left temporal and parietal metabolism. Further, left temporal FA correlated with left prefrontal metabolism. Finally, bilateral parietal FA correlated with bilateral temporal metabolism. Interestingly, more unilateral FA-metabolic associations were observed in the left hemisphere. To elucidate the potential importance of regional white matter FA, we regressed total white matter FA with metabolism. The same regions continually appear with low FA correlating to decreased metabolism (bilateral cuneus and insula, and left calcarine, precuneus, and lingual regions). This suggests the global mean FA measure is similar to the regional FA evaluations, however we did not find prefrontal metabolic associations with the global FA analysis. Therefore regional FA can aid in elucidating more regionally specific changes when investigating FA-metabolic associations.

The major white matter tracts that seem to be associated with metabolism are the longitudinal fasciculus and those associated with fronto-temporal connectivity. The superior longitudinal fasciculus (SLF) runs the span of the prefrontal cortex to the parietal lobe and the inferior longitudinal fasciculus connects the temporal to posterior brain regions. The SLF subdivides into four distinct components, SLFI, SLFII, SLFIII, and the arcuate fasciculus. Briefly, SLFI primarily connects the superior parietal to the premotor and prefrontal cortices, SLFII connects the inferior parietal to the dorsal premotor and prefrontal cortices, and the SLFIII connects the ventral parietal to ventral premotor and prefrontal cortices [35]. Consistent with these known SLF relationships, our data illustrate lower FA in IFWM and MFWM is associated with parietal lobe hypometabolism, whereas the prefrontal FA relationship with temporal regional metabolism is most likely reflected via the complex fronto-temporal associations. The fronto-temporal associations are more complex and less understood. Several studies now show functional connectivity between frontal and temporal regions using functional imaging [21, 23,24] and the combination of functional and tensor imaging [22]. Most notably, the cingulum bundle connects the posterior cingulate cortex/retrosplenial cortex (PCC/RSC) to the medial prefrontal cortex. Further, the caudal regions of the PCC/RSC also connect to the medial temporal region. Although the temporal and prefrontal regions have yet to reveal direct inter-connecting white matter pathways, there are likely to be pathways for information transfer between the two regions. Therefore, the parietal associations with both frontal and temporal areas may be indicative of SLF alterations, while the fronto-temporal relationships are probably a combination of white matter pathways, possibly those discussed earlier [21–24]. While there are numerous white matter tracts that are putatively affected by aging and disease, DTI is most likely detecting the larger white matter bundles. As technology improves, our ability to detect the contributions of smaller white matter tracts will further aid in our understanding of the relationships between white and gray matter changes.

Both grey and white matter structures are crucial for cognition. Our data reveal associations between gray matter metabolism and white matter integrity in regions associated with specific cognitive function. The left prefrontal cortex is proposed to be involved in the encoding of novel information into episodic memory [36]. Further, the temporoparietal regions are

associated with specific cognitive tasks, such as the hippocampus being associated with episodic memory [37] and the parietal regions associated with sensory function but also episodic memory [38,39]. Our data show correlations between white matter integrity and gray matter metabolism for the prefrontal cortex, temporal and parietal regions. Importantly, these regions are also associated with the cognitive processes affected in AD and CVD, suggesting a link with white matter degeneration and gray matter hypometabolism.

As noted previously, there are more FA associations with the left hemisphere. Our FDG-PET regression analysis with MMSE revealed a predominant left hemispheric hypometabolism, which would consequently affect our FA associations. Left hemispheric dominance, especially within the temporoparietal regions, has been observed in many metabolic studies and is obviously dependent on the composition of the cohort and, when relevant, the covariate used in the analysis [15,40,41]. Our metabolic correlations with MMSE also support our restricted FA associations between the left IFWM and temporal regions. The left IFWM FA associations with the temporal regions but not with proximal frontal regions are probably due to the preservation of frontal metabolism in this cohort. There is a small region in the left prefrontal cortex that correlates to MMSE, however the frontal regions are quite preserved with respect to metabolism. This is not surprising as frontal hypometabolism is usually observed in progressed AD and therefore, we suspect is not prevalent enough in this sample to correlate with the FA of the frontal lobe. Lastly, we did investigate between group FA differences across white matter ROI's. As anticipated, the trend of FA values was AD < CIND < Normal. Due to the insufficient sample sizes for between group analyses, we have restricted our interpretation to represent trends and will not further speculate on these results.

We do note the striatum and thalamic regions correlated with some white matter ROI's. These subcortical regions are atrophic in dementia, and may be in close proximity to lacunar infarctions. In addition, the thalamus has numerous divergent cortical projections. These are potential reasons that may explain the subcortical-cortical correlations within this cohort.

Our corpus callosum data correspond well with the current literature, in that, the posterior region was more associated with larger areas of metabolic change [8,11]. The splenium had the greatest association with metabolic decline. This is in concert with the numerous parietal, occipital and temporal regional associations and is not surprising as the posterior portion of the brain is more affected in AD.

There are at least two possible interpretations of these results. First, the degeneration of neuronal cell bodies causes reduced metabolism in the affected gray matter region and that the degradation of associated axons is responsible for the decreased fractional anisotropy detected in the associated white matter tracts. An alternative interpretation is that the pathology begins in the white matter tracts, and that disconnection between cortical regions is responsible for reduced glucose uptake. The first interpretation would support the underlying pathology of AD, with gray matter changes or atrophy causing white matter alterations. While the second interpretation would support the underlying pathology of CVD, with white matter changes causing gray matter alterations. In this study we had neither the sample size nor all of the data necessary to convincingly test these alternative explanations, however, our data provide evidence of the complex and intriguing relationship between white matter integrity and gray matter function.

The major limitation of this study is the small sample size. However, the correlations we have shown are relatively strong and we hope this will initiate more studies of white matter integrity and metabolism. Another limitation is the multiple comparisons of this voxel based study limit interpretation of the results. Although we did not correct for multiple comparisons, we did restrict our findings to a cluster size of 100 or larger. This inhibits finding smaller significant

areas, but it minimizes the chance of type I error. Because our results revealed large areas previously associated with CVD and AD, it seems unlikely that they are a consequence of false discovery. It is possible that the FA-metabolic correlations could be due to individual trends (i.e. white and gray matter alterations that are not related and just coincident events or trends within the dataset) rather than reflecting coherent relationships, thus we anticipate future studies will aid in our understanding of how metabolism and white matter potentially interact in aging and dementia. A further limitation of this study results from the need to coregister the DTI to the T1 image. The DTI images were acquired using an echoplanar sequence which has considerably more geometric distortion than the T1 image; thus, there may not be exact correspondence between the DTI and T1 images. To address this limitation, we drew small regions in the white matter for the parietal and temporal regions directly on the DTI image. These regions could be drawn with relative reliability on the DTI, where we were unable to reliably draw the IFWM and MFWM. We then extracted the FA data from the parietal and temporal DTI regions of interest and used them in the same SPM analyses as we did with the original T1 ROI's. The resulting significant regions were extremely similar and did not alter our overall results. This confirms the distortion, in our sample, was negligible and the T1 ROI's were appropriately placed on the DTI post coregistration. Finally, DTI is a relatively new imaging technique and will aid in elucidating disease progression as the technology continues to improve. We anticipate this paper will initiate more investigations of white matter tracts and associated regional metabolism.

Our data reveal as white matter tracts degenerate, associated cortices also show lower metabolism. Therefore, white matter integrity and gray matter metabolism are intimately associated. This association is probably based on several factors such as a loss of white matter innervation to the gray matter, or loss of cortical neurons and axons resulting in white matter degeneration. The relationships are interesting but complex, and with further investigation these associations could facilitate our understanding of aging and neurodegeneration.

Acknowledgments

The authors thank Drs Charles De Carli and Christine Nordahl for the creation of the MDT2 template used in our analyses. We would also like to thank Dr. Lothar Schad from the German Cancer Research Center and University of Heidelberg for providing the DTI sequence and Dr. Geon-Ho Jahng from Kyung-Hee, University Seoul and Dr. Norbert Schuff from the University of California, San Francisco for refining the sequence to guarantee quality DTI data.

Funding

National Institute of Aging AG12435

References

1. Du AT, et al. White matter lesions are associated with cortical atrophy more than entorhinal and hippocampal atrophy. Neurobiol Aging 2005;26(4):553–9. [PubMed: 15653183]
2. Reed BR, et al. Effects of white matter lesions and lacunes on cortical function. Arch Neurol 2004;61 (10):1545–50. [PubMed: 15477508]
3. Tullberg M, et al. White matter lesions impair frontal lobe function regardless of their location. Neurology 2004;63:246–253. [PubMed: 15277616]
4. Nordahl CW, et al. White matter changes compromise prefrontal cortex function in healthy elderly individuals. J Cogn Neurosci 2006;18(3):418–29. [PubMed: 16513006]
5. Nusbaum AO, et al. Regional and global changes in cerebral diffusion with normal aging. AJNR Am J Neuroradiol 2001;22(1):136–42. [PubMed: 11158899]
6. Salat DH, et al. Age-related alterations in white matter microstructure measured by diffusion tensor imaging. Neurobiol Aging 2005;26(8):1215–27. [PubMed: 15917106]
7. Hanyu H, et al. Diffusion-weighted MR imaging of the hippocampus and temporal white matter in Alzheimer's disease. J Neurol Sci 1998;156(2):195–200. [PubMed: 9588857]

8. Hanyu H, et al. Diffusion-weighted and magnetization transfer imaging of the corpus callosum in Alzheimer's disease. J Neurol Sci 1999;167(1):37–44. [PubMed: 10500260]
9. Rose SE, et al. Loss of connectivity in Alzheimer's disease: an evaluation of white matter tract integrity with colour coded MR diffusion tensor imaging. J Neurol Neurosurg Psychiatry 2000;69(4):528–30. [PubMed: 10990518]
10. Sandson TA, et al. Diffusion-weighted magnetic resonance imaging in Alzheimer's disease. Dement Geriatr Cogn Disord 1999;10(2):166–71. [PubMed: 10026392]
11. Takahashi S, et al. Selective reduction of diffusion anisotropy in white matter of Alzheimer disease brains measured by 3.0 Tesla magnetic resonance imaging. Neurosci Lett 2002;332(1):45–8. [PubMed: 12377381]
12. Teipel SJ, et al. Multivariate network analysis of fiber tract integrity in Alzheimer's disease. Neuroimage 2007;34(3):985–95. [PubMed: 17166745]
13. Zhang Y, et al. Diffusion tensor imaging of cingulum fibers in mild cognitive impairment and Alzheimer disease. Neurology 2007;68(1):13–9. [PubMed: 17200485]
14. Drzezga A, et al. Cerebral glucose metabolism in patients with AD and different APOE genotypes. Neurology 2005;64:102–107. [PubMed: 15642911]
15. Kuczynski B, Reed B, Mungas D, Weiner M, Chui H, Jagust W. Cognitive and anatomic contributions of metabolic decline in Alzheimers and Cerebrovascular Disease. Arch Neurol 2008;65(5):650–5. [PubMed: 18474742]
16. Kwan LT, et al. Effects of subcortical cerebral infarction on cortical glucose metabolism and cognitive function. Arch Neurol 1999;56:809–814. [PubMed: 10404982]
17. Mosconi L, et al. MCI conversion to dementia and the APOE genotype A prediction study with FDG-PET. Neurology 2004;63:2332–2340. [PubMed: 15623696]
18. Nobili F, et al. Resting SPECT-neuropsychology correlation in very mild Alzheimer's disease. Clinical Neurophysiology 2005;116:364–375. [PubMed: 15661114]
19. Wu CC, et al. Imaging interactions between Alzheimer's Disrase and Cerebrovascular Disease. Ann NY Acad Sci 2002;977:403–410. [PubMed: 12480779]
20. de Jong LW, et al. Strongly reduced volumes of putamen and thalamus in Alzheimer's disease: an MRI study. Brain 2008;131(Pt 12):3277–85. [PubMed: 19022861]
21. Villain N, et al. Relationships between hippocampal atrophy, white matter disruption, and gray matter hypometabolism in Alzheimer's disease. J Neurosci 2008;28(24):6174–81. [PubMed: 18550759]
22. Greicius MD, et al. Resting-state functional connectivity reflects structural connectivity in the default mode network. Cereb Cortex 2009;19(1):72–8. [PubMed: 18403396]
23. Allen G, et al. Reduced hippocampal functional connectivity in Alzheimer disease. Arch Neurol 2007;64(10):1482–7. [PubMed: 17923631]
24. Wang L, et al. Changes in hippocampal connectivity in the early stages of Alzheimer's disease: evidence from resting state fMRI. Neuroimage 2006;31(2):496–504. [PubMed: 16473024]
25. Grady CL, et al. Altered brain functional connectivity and impaired short-term memory in Alzheimer's disease. Brain 2001;124(Pt 4):739–56. [PubMed: 11287374]
26. Fein G, et al. Hippocampal and cortical atrophy predict dementia in subcortical ischemic vascular disease. Neurology 2000;55:1626–1635. [PubMed: 11113215]
27. Mungas D, et al. MRI predictors of cognition in subcortical ischemic vascular disease and Alzheimer's disease. Neurology 2001;57:2229–2235. [PubMed: 11756602]
28. Morris JC. Clinical dementia rating: a reliable and valid diagnostic and staging measure for dementia of the Alzheimer type. Int Psychogeriatr 1997;9(Suppl 1):173–6. discussion 177–8. [PubMed: 9447441]
29. Chui HC, et al. Clinical criteria for the diagnosis of vascular dementia: a multicenter study of comparability and interrater reliability. Arch Neurol 2000;57(2):191–6. [PubMed: 10681076]
30. McKhann G, et al. Clinical diagnosis of Alzheimer's disease: report of the NINCDS-ADRDA Work Group under the auspices of Department of Health and Human Services Task Force on Alzheimer's Disease. Neurology 1984;34(7):939–44. [PubMed: 6610841]
31. Chui HC, et al. Cognitive impact of subcortical vascular and Alzheimer's disease pathology. Ann Neurol 2006;60(6):677–87. [PubMed: 17192928]

32. Meltzer CC, et al. Correction of PET data for partial volume effects in human cerebral cortex by MR imaging. J Comput Assist Tomogr 1990;14(4):561–70. [PubMed: 2370355]

33. Sun FT, et al. Automated template-based PET region of interest analyses in the aging brain. Neuroimage 2007;34(2):608–17. [PubMed: 17112749]

34. Jiang H, et al. DtiStudio: resource program for diffusion tensor computation and fiber bundle tracking. Comput Methods Programs Biomed 2006;81(2):106–16. [PubMed: 16413083]

35. Schmahmann JD, et al. Association fibre pathways of the brain: parallel observations from diffusion spectrum imaging and autoradiography. Brain 2007;130(Pt 3):630–53. [PubMed: 17293361]

36. Blanchet S, et al. New questions on the hemispheric encoding/retrieval asymmetry (HERA) model assessed by divided visual-field tachistoscopy in normal subjects. Neuropsychologia 2001;39(5): 502–9. [PubMed: 11254932]

37. Manns JR, Eichenbaum H. Evolution of declarative memory. Hippocampus 2006;16(9):795–808. [PubMed: 16881079]

38. Cabeza R, Nyberg L. Neural bases of learning and memory: functional neuroimaging evidence. Curr Opin Neurol 2000;13(4):415–21. [PubMed: 10970058]

39. Berryhill ME, et al. Parietal lobe and episodic memory: bilateral damage causes impaired free recall of autobiographical memory. J Neurosci 2007;27(52):14415–23. [PubMed: 18160649]

40. Kalpouzos G, et al. Working memory and FDG-PET dissociate early and late onset Alzheimer disease patients. J Neurol 2005;252(5):548–58. [PubMed: 15726251]

41. Teipel SJ, et al. Resting state glucose utilization and the CERAD cognitive battery in patients with Alzheimer's disease. Neurobiol Aging 2006;27(5):681–90. [PubMed: 15908048]

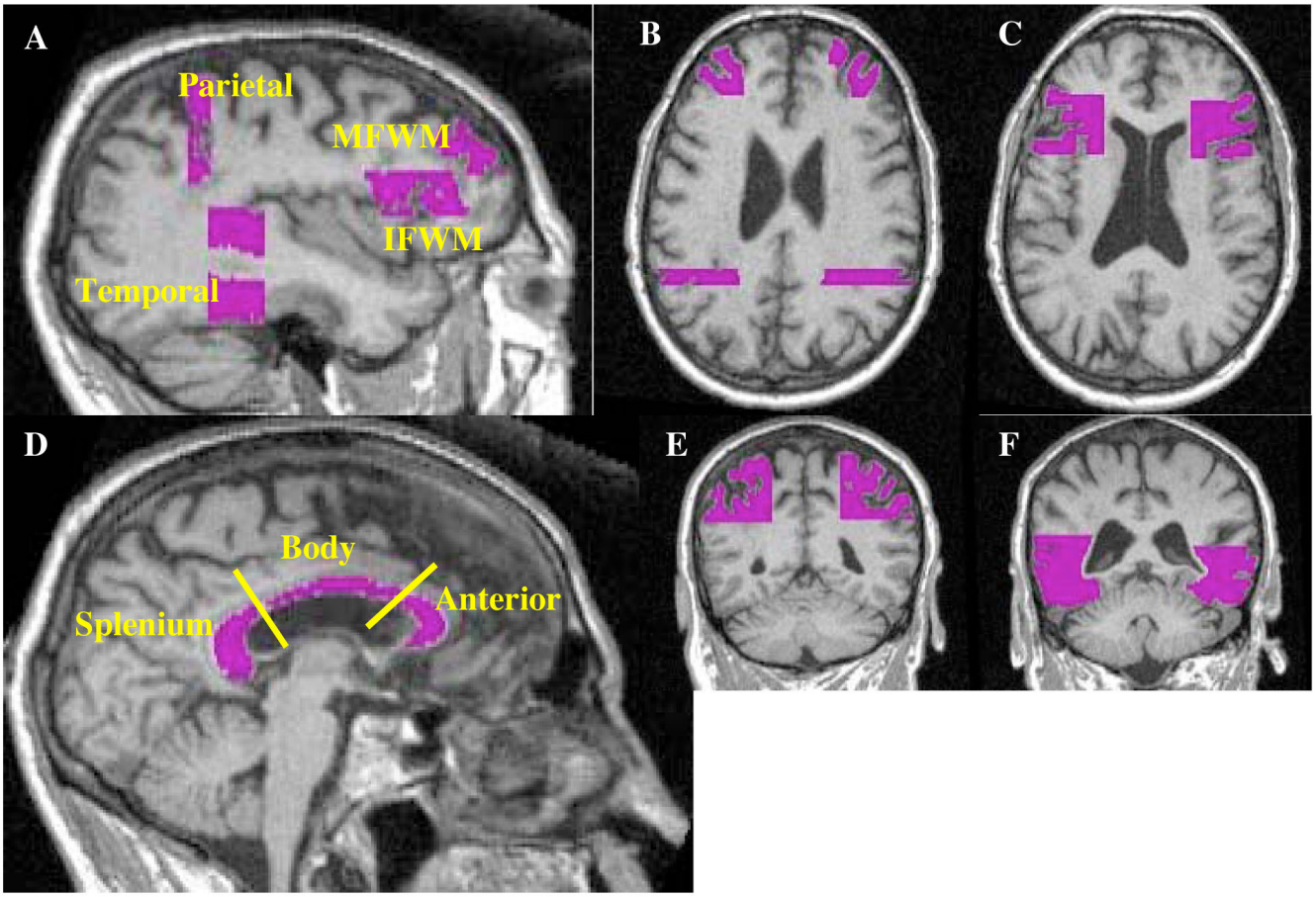

Figure 1.

Represents the white matter regions of interest (ROI) using a single subject for display in which a). displays all of the lobar ROI's, b). displays the axial view of the MFWM and temporal ROI's, c). displays the axial view of the IFWM, while the coronal views of the parietal and temporal ROI's are depicted in e and f, respectively. The corpus callosum ROI's, which were divided into three separate regions, the splenium, body and anterior portions are displayed in d.

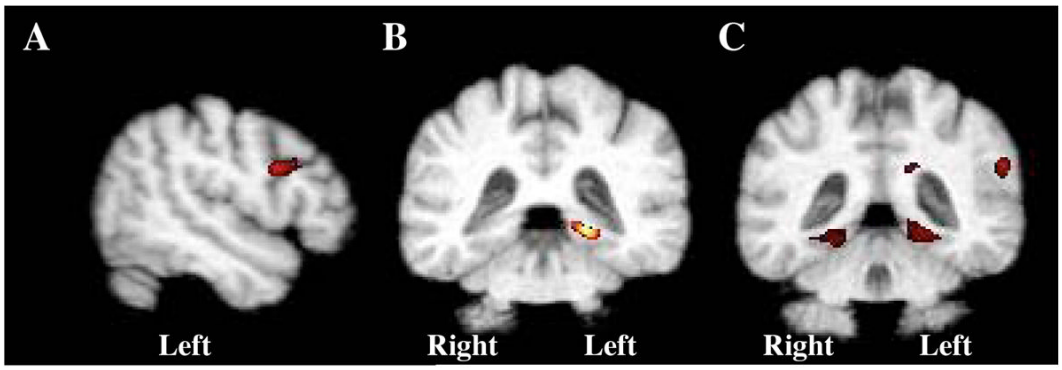

Figure 2.
Results illustrated on the MDT2 template depicting a). left temporal b). left IFWM and c). left parietal FA values positively regressed with FDG-PET, ($p \leq 0.005$, uncorrected; N=16). Regions shown are a). left IFWM, b). left parahippocampal gyrus and c). bilateral lingual, and parahippocampal gyri and the left supramarginal gyrus.

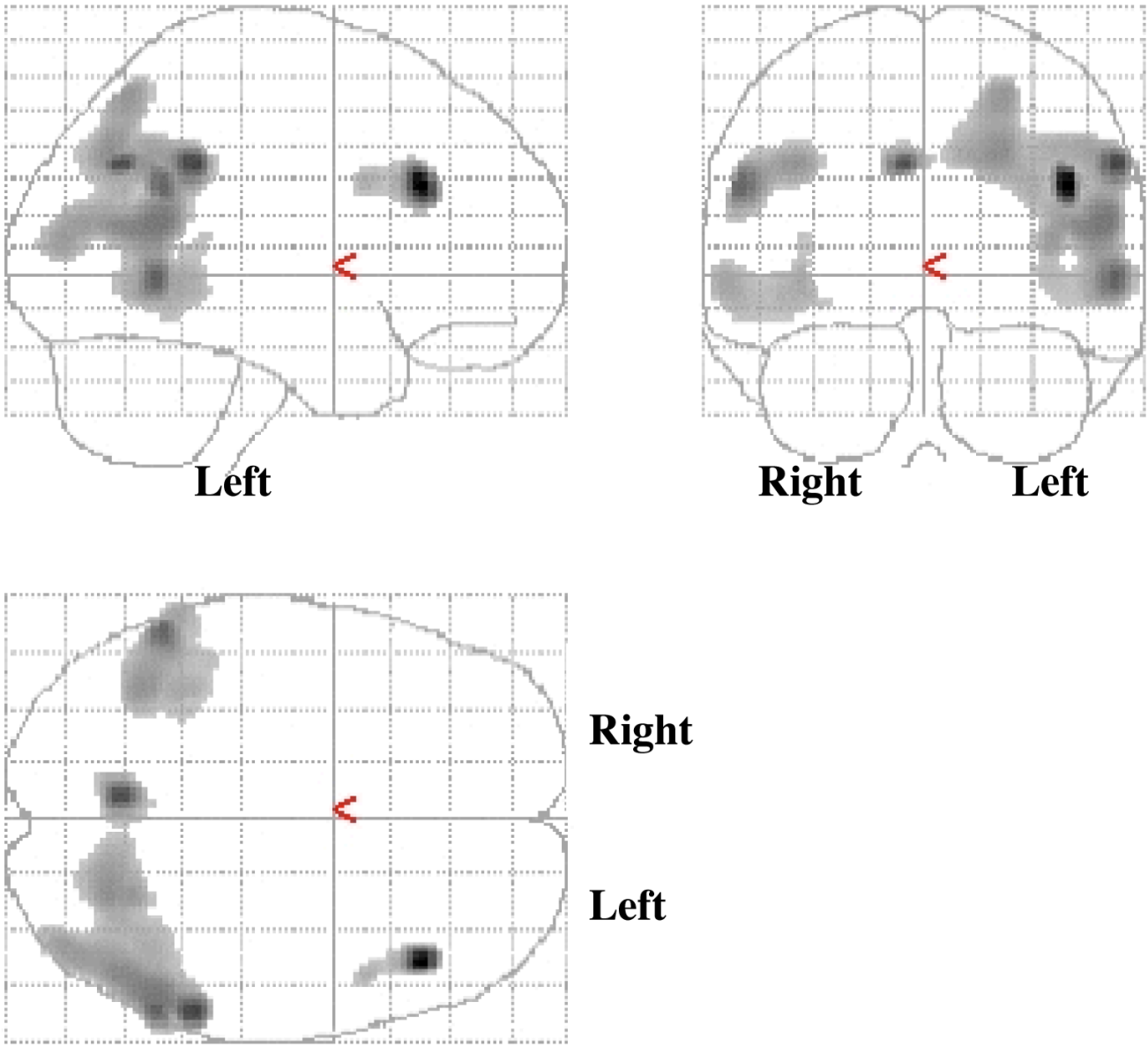

Figure 3.
Represents the results from a regression analysis between FDG-PET and MMSE, controlled by age ($p < 0.001$; voxel cluster > 100), displayed on the SPM glass-brain.

Table 1

Subject Characteristics (N=16; Values are Mean (SD))

Characteristics	CN	CIND	D	Total
Men/Women	3/1	3/2	3/4	9/7
Age	73.3 (7.1)	79.8 (8.4)	77.7 (5.3)	77.3 (6.8)
Education	15.0 (3.5)	12.8 (1.1)	13.7 (3.2)	13.8 (2.7)
MMSE	28.3 (1.7)	26.0 (4.0)	17.1 (8.5)*	22.7 (7.7)

*denotes a significant difference from CN and CIND groups $p < 0.05$; CN = Cognitively Normal, CIND = Cognitively Normal Not Demented, and D = Demented

Table 2

Brain Regions showing significant unilateral correlations (p<0.005, cluster size>100) with Regional FA values

Region of Interest (White Matter)	Correlated Gray Matter Region (Glucose Metabolism)	MNI Coordinates
MFWM-Left	Left Supramarginal Gyrus	−62, −32, 33
	Left Superior Temporal Gyrus	−50, −2, −1
	Left Insula	−49, −2, 0
	Left Angular Gyrus	−41, −68, 44
	Left Middle Occipital Gyrus	−40, −73, 29
MFWM-Right	Right Cuneus	8, −78, 31
IFWM-Left	Left Angular	−36, −71, 41
	Left Middle Occipital Gyrus	−37, −69, 40
	Left Parahippocampal Gyrus	−29, −37,−5
	Left Lingual Gyrus	−16, −43, −3
IFWM-Right	No unilateral associations	
Temporal-Left	Left Insula	−41, −4, 0
	Left Thalamus	−5, −12, 3
	Left Frontal Inferior Opercularis	−54, 11, 24
Temporal-Right	Right Cuneus	13, −82, 31
	Right Superior Occipital Gyrus	17, −82, 32
Parietal-Left	Left Calcarine	−23, −62, 13
	Left Lingual Gyrus	−20, −43, −7
	Left Supramarginal Gyrus	−64, −28, 24
	Left Insula	−43, 0, 3
	Left Parahippocampal Gyrus	−20, −43, −4
	Left Precuneus	−25, −55, 23
	Left Insula	−47, 0, −1
	Left Thalamus	−9, −16, 7
Parietal-Right	Right Thalamus	9, −16, 7
	Right Cuneus	9, −76, 29
	Right Hippocampus	36, −28, −7
	Right Parahippocampal Gyrus	23, −39, −8

Table 3

Corpus Callosum Regions showing significant correlations ($p<0.005$, cluster size>100) with Regional FA values

Region of Interest (White Matter)	Correlated Gray Matter Region (Glucose Metabolism)	MNI Coordinates
Anterior-Left	Left Calcarine	−16, −50, 12
	Left Lingual Gyrus	−19, −50, 1
Anterior-Right	No unilateral associations	
Body-Left	Left PostCentral Gyrus	−50, −23, 44
	Left PreCentral Gyrus	−48, −16, 45
Body-Right	Right Hippocampus	28, −30, −3
	Right Thalamus	17, −25, 5
	Right Calcarine	16, −60, 15
Splenium-Left	Left Paracentral Lobule	−9, −34, 70
	Left Superior Temporal Gyrus	−66, −28, 17
	Left Rolandic Opercularis	−49, 2, 4
	Left Insula	−41, 2, 4
	Left Superior Frontal Gyrus	−17, 41, 45
Splenium-Right	Right Lingual Gyrus	21, −43, −4
	Right Parahippocampal Gyrus	25, −41, −7
	Right Hippocampus	33, −32, −1
	Right PreCentral Gyrus	41, −16, 58
	Right PostCentral Gyrus	45, −16, 53